RSC Advances

Synthesis and magnetostructural studies of amine functionalized superparamagnetic iron oxide nanoparticles

Journal:	*RSC Advances*
Manuscript ID:	RA-ART-01-2015-000049.R1
Article Type:	Paper
Date Submitted by the Author:	04-Feb-2015
Complete List of Authors:	Salunkhe, Ashwini; Savitribai Phule Pune University, Pune, Department of Physics Khot, Vishwajeet; D. Y. Patil University,, Centre for Interdisciplinary Research Ruso, Juan; University of Santiago de Compostela, Applied Physics Patil, Shankar; University of Pune, Department of Physics

Synthesis and magnetostructural studies of amine functionalized superparamagnetic iron oxide nanoparticles

A. B. Salunkhe[1], V. M. Khot[2], J. M. Ruso[3], S. I. Patil[1*]

[1*] Advanced materials processing lab, Department of Physics, Savitribai Phule Pune University, Pune, Maharashtra, INDIA, 411007 Email Add: patil@physics.unipune.ac.in, Phone (Office): +91 20 25601420 (Fax): +91 20 25691684

[2] Center for Interdisciplinary Research, D. Y. Patil University, Kolhapur-416006, Maharashtra, India

[3]Soft matter and molecular biophysics group, Applied Physics Department, University of Santiago de Compostela, Santiago de Compostela, SPAIN

Abstract

Superparamagnetic iron oxide nanoparticles are synthesized through the co precipitation method by using new generation base Diisopropylamine (DIPA) which electrostatically complexes with the iron ions, reduces them and subsequently caps the nanoparticles. Coating of DIPA on the surface of nanoparticles was confirmed through FTIR and TG-DTA. We investigate the effect of reaction time as well concentration of DIPA on the particle size and magnetic properties of Fe_3O_4 nanoparticles. The effect of concentration of DIPA on particle size reveals that, the nanocrystallite size of Fe_3O_4 nanoparticles increases to maximum (increase is nominal 5.2 nm to 8.5 nm) and then reduces (3.2 nm). The particle size and magnetic properties of synthesized nanoparticles are also influenced by the reaction time, in general as reaction time increases the particle size increases. The lattice parameter of iron oxide nanoparticles is varied from ~8.32 to ~8.39 Å with reaction time. From magnetic measurements, superparamagnetism in Fe_3O_4 nanoparticles was confirmed. The results clearly suggest that the magneto-structural properties of Fe_3O_4 (or any ferrite) can be easily tuned by using DIPA.

Keywords: Magnetic nanoparticles, aqueous co-precipitation method, Size-controlled magnetite, Superparamagnetic behavior

Introduction

Iron oxide magnetic nanoparticles (MNPs) are one of the most accepted multifunctional magnetic materials with diverse applications including high density magnetic storage[1]multi-tera bit storage [2], catalysis [3], sensors[4], environmental remediation[5] and in biomedicine [6,7] with a platform for high sensitivity bimolecular Magnetic Resonance Imaging (MRI) [8]. For these applications iron oxide nanoparticles (NPs) usually used as a core surrounded by a hydrophilic and biocompatible coatings mostly polymers. But there is main limitation to use conventionally synthesized and polymer functionalized Fe_3O_4 NPs for biomedical application due to the presence of a thick layer that increases the hydrodynamic radii considerably (up to 100 nm), causing the damping of the MR signal. This limitation can be overcome by introduction of cationic surface layer on the top of iron oxide NPs such as amine (NH_2). Amine functionalized iron oxide NPs surface is supposed to have very good uptake by cancer cells and provide sharper in vivo and in vitro MRI signals as compared to conventional iron oxide NPs [9,10]. However along with surface functionalization, required physicochemical and magnetic properties of iron oxide NPs can be tailored merely during synthesis process. Large scale application and tailoring of various physico-chemical properties of iron oxide NPs have prompted the development of several widely used methods including combustion synthesis, micro-emulsion, hydrothermal, reverse micelle, sol gel technique, sonochemical synthesis, citrate precursor technique, microwave plasma, mechanical alloying, co precipitation etc for the fabrication of stoichiometric and chemically pure spinel ferrites NPs [11,12].

Among these various synthesis methods, the aqueous co-precipitation route is mostly used method for producing water dispersible MNPs in high yields, since it is cost- effective, less time consuming and easily scalable for industrial as well as pharmaceutical applications. Along with this, for co-precipitation route there is no need of expensive and hazardous solvents, reagents and high temperature or pressure [13-15]. Ultimately, co-precipitation synthesis in water based system represents a beneficial method and eco friendly synthesis method. Even though co-precipitation technique is most studied and most familiar synthesis method, the control of magnetic properties and crystallinity of NPs synthesized by this route is still needed to be studied thoroughly [16,17]. Even surprising researchers were working extensively on water based co precipitation synthesis technique; maximum work was carried out with the traditional bases (sodium hydroxide, ammonia, and tetra alkylammonium hydroxides). Pereirra et al have studied

the different bases like NaOH, NH_4OH, isopropanolamine (MIPA), diisopropanolamine (DIPA) etc. and the role played by the bases on the particles' size, chemical composition, and magnetic properties on Fe_3O_4 NPs. Their results supports that, MIPA and DIPA have an important role on the co-precipitation process since they acted as the base and at the same time as a complexing agent that control the growth of NPs and provides higher surface spin order. Their results shed new light on the design of MNPs with improved properties through the co precipitation method [13]. Still it is well known that, the reaction conditions may affect the particle properties with which one can customize MNPs for variety of applications.

In this context in the present investigation, we adopted a new approach to describe and predict the impact of the main synthesis parameters in co-precipitation method on the properties of synthesized MNPs. We chose reaction time and concentration of alkaline media (DIPA) as a parameters of interest. All syntheses were carried out in a well defined and controlled reaction setup. Magnetic properties of synthesized MNPs were measured by a superconducting quantum interference device (SQUID) and crystallographic and chemical properties by TGA, XRD, FTIR and TEM etc.

Experimental:

Materials and reagents: Ferrous chloride tetrahydrate (≥99%), Ferric chloride hexahydrate (≥99%), bis(2-hydroxypropyl)-amine (DIPA, ≥98%), were purchase by Sigma Aldrich. Hydrochloric acid (analytical grade) was by Panreac and was used for the synthesis purpose. Double distilled water used throughout the experiments. All reagents were used without further purification

Synthesis: MNPs were prepared by the aqueous co-precipitation method under alkaline conditions using DIPA as the base. In which, 20 mmol of $FeCl_3 \cdot 6H_2O$ and 10 mmol of $FeCl_2 \cdot 4H_2O$ were dissolved in 25 cm^3 of deoxygenated 0.5 M HCl solution. This solution was quickly added to 250 cm^3 of a deoxygenated 3.0M solution of DIPA (pH 11−12) at room temperature with vigorous mechanical stirring. A black precipitate formed immediately and stirring was continued for 2 h. The precipitate was magnetically separated, washed with deoxygenated water several times. After washing obtained precipitate was dried at room temperature.

Particles were prepared at different reaction times of ½, 1 and 2 h. The other parameters such as reagent concentrations, reaction temperature and the stirrer speed (1200 RPM) were kept constant. Particles are also prepared with different alkali concentration of 3.0, 5.0, 7.0 M. We denoted the prepared samples as N3½, N31, N32, N5½, N51, N52, N7½, N71, N72 for 3.0, 5.0, 7.0M concentration with ½, 1 and 2 h reaction time respectively. In this nomenclature, 'N' is stands for nanoparticles, First numeric is for normality while second numeric is for reaction time in hours.

Physico-chemical Characterization:

Structure and phase of as synthesized Fe_3O_4 NPs was studied by XRD (miniflex 600) with Cu-Kα radiation (λ=1.5404 Å) in the 2θ range from 20 to 80°. The patterns were evaluated by Panalytical X'pert high score software and compared with standard JCPDS (card no. 19-0629). Presence of the magnetic core and ligands on the surface of MNPs was confirmed by FTIR spectroscopy (Perkin Elmer spectrometer model no. 783, USA). The particle size of Fe_3O_4 NPs was measured with TEM (Philips CM 200 model, operating voltage 20–200 kV, resolution 2.4 Å). The magnetic properties of the dried MNPs were studied using a commercial Quantum Design superconducting quantum interference device (SQUID) magnetometer. The isothermal magnetization (M) versus applied magnetic field (H) at an applied field of ±15 kOe at room temperature and ZFC-FC measurements were performed over the temperature range 5−370 K with constant field 100 Oe.

Results and discussion:

Reaction mechanism

In the synthesis of NPs/nanomaterials, the crystal structure, shape, size and size distribution is mainly controlled by crystallization process (Nucleation and Growth). A theoretical approach to understand the mechanism of crystal formation provides a greater control over the size, shape and composition of nanocrystals and controlled size which helps to tune the above mentioned properties by varying the crystallization conditions.

In co-precipitation technique, the new phase formed when the temperature of the solute decreases below phase formation point and the concentration of solute in a solvent exceed its equilibrium solubility or supersaturated. Such supersaturated solutions have high Gibbs free

energy and the overall energy of the system would be reduced by segregating solute from the solution. This reduction of Gibbs free energy is the driving force for both nucleation and growth. The Gibbs free energy per unit volume of the solid phase (ΔG_v) is dependent on the concentration of the solute and is given as,

$$\Delta G_v = -kT/\Omega \ln(C/C_o) = -kT/\Omega \ln (1+\sigma) \quad (1)$$

Where, C and Co are the concentrations of the solute and the equilibrium concentration or solubility respectively, σ is the supersaturation (defined by $(C-C_o)/C_o$) and Ω is the atomic volume. If σ is zero, ΔG_v would be zero means there is no nucleation would occur without supersaturation. When the concentration of solute exceeds than the equilibrium concentration ($C > C_o$), the ΔG_v becomes negative and nucleation occurs spontaneously. After nucleation the newly formed nucleus is stable only when its radius exceeds a critical size, r* which is given by,

$$r^* = -2\gamma / \Delta G_v \quad (2)$$

where γ is the surface energy per unit area. However, a nucleus smaller than r* will dissolve into the solution to reduce the overall free energy, whereas a nucleus larger than r* is stable and continues to grow bigger. At the critical size r = r*, $d\Delta G/dr = 0$, critical energy, ΔG*, is defined by,

$$\Delta G^* = 16\pi\gamma/3(\Delta G_v)^2 \quad (3)$$

ΔG* is the energy barrier that a nucleation process must overcome. The critical size represents the limit how small NPs can be synthesized by nucleation from supersaturated solution. If the concentration of solute increases as a function of time, no nucleation would occur even above equilibrium solubility. When the supersaturation reaches to a certain value above the solubility the nucleation occurs, which corresponds to the energy barrier for the formation of nuclei. (Fig. 1) (eq. $\Delta G^* = 16\pi\gamma/3(\Delta G_v)^2$) However, the growth of the particles can continue through nuclear addition until the concentration of precipitated species reaches to an equilibrium concentration.[18] When the critical size r* is smaller than the particle size of synthesized particles r, ($r > r^*$) the smaller particles grow more rapidly than the larger ones because smaller particles have more free energy driving force compared to larger ones and this is the stage where nearly monodisperse size distribution can be obtained by stopping the reaction. Whereas, the increase in critical nuclei

size (r*) due to decrease in supersaturation ratio there is occurrence of ripening process [19]. After the growth phase the terms agglomeration and aging are used to describe features of the changes in the solid particles. Tendency of smaller particles in a liquid suspension to coalesce into larger aggregates is nothing but agglomeration. The other variety of processes that changes a precipitate after its formation are covers under the title aging. For example: Ostwald ripening i.e. the tendency of larger crystals to cultivate at the expense of smaller crystals when the crystals formed after nucleation. Another crucial process which transforms with aging is initial nucleation of a metastable solid phase, which can be well understood with the example of amorphous solid particles that crystallize with time of a hydrated crystalline solid that converts to a more stable material [20].

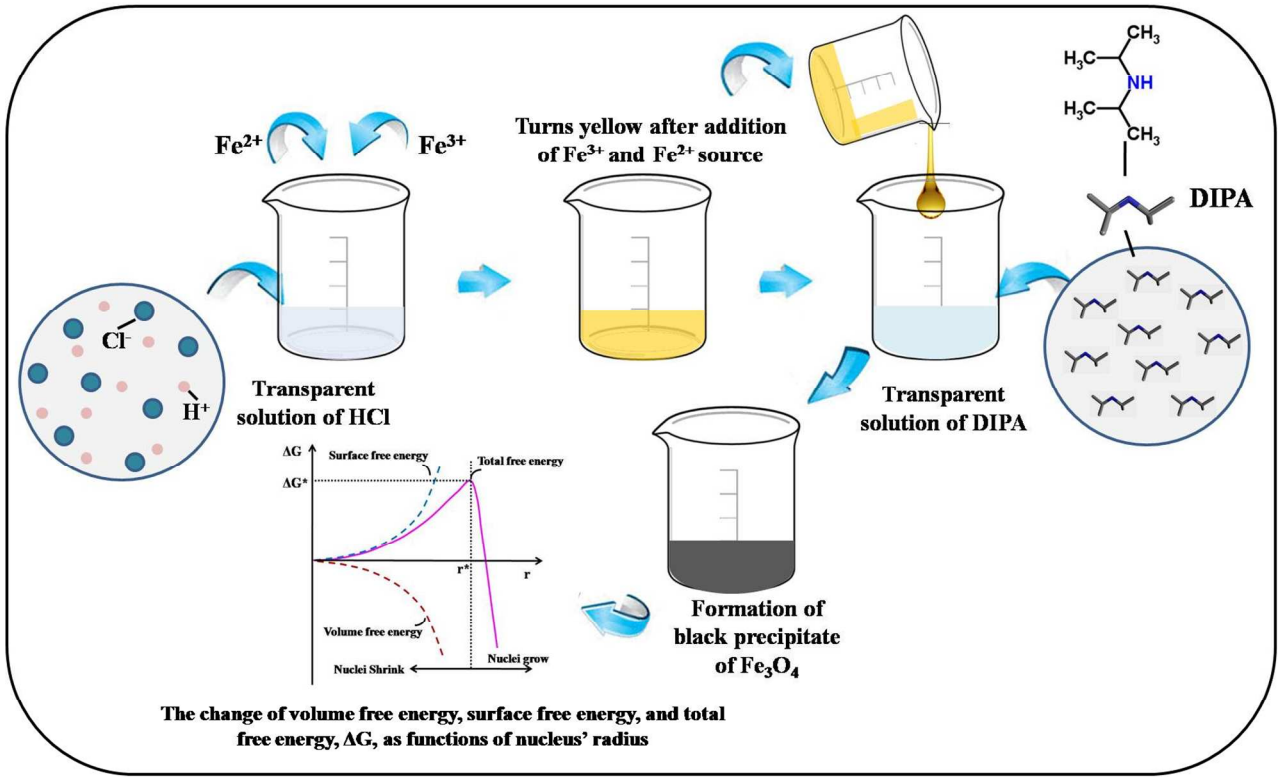

Fig. 1 Synthesis of Iron oxide Nanoparticles by co precipitation method

Basically, co-precipitation process consists of a condensation reaction in which cations present in the solution bond together through oxygenated bridges, such as OH or O_2. It begins by the initiation of monomer species, such as M–OH, whose concentration increases rapidly with the base addition. Then, the precipitated hydroxide converts to the oxide by replacement of the hydroxide bridges by oxygen bonds. In the present investigation, the co precipitation carried with

alkanolamines, in which Fe_3O_4 NPs nucleated by simultaneous hydrolysis and dehydration of a mixture of divalent and trivalent iron salt solution. The ratio of concentration of Fe^{3+} and Fe^{2+} salts were kept constant and salt solutions were prepared in acidic matrix so as to avoid formation of iron hydroxides before initiation of reaction. In acidic medium (at pH 3), the first phase of Fe^{3+} to precipitate in hydrolysis is ferrihydrite. The magnetite forms after addition of alkanolamine (base) on increasing pH, the divalent Fe^{2+} integrate in to the ferrihydrite and forms an intermediate complex material of Fe^{2+}- ferrihydrite and later compensates as inverse spinel structured magnetite. The overall chemical reaction can be expressed as,

$$2Fe^{3+} + Fe^{2+} + 8OH^- = \mathrm{FeO.Fe_2O_3} + 4\mathrm{H_2O} \quad (3)$$

The basicity of the alkanolamines is lower as compared to the old generation bases (NaOH, NH_4OH etc) which help to reduce particle size of the NPs.

Structural and Phase Analysis

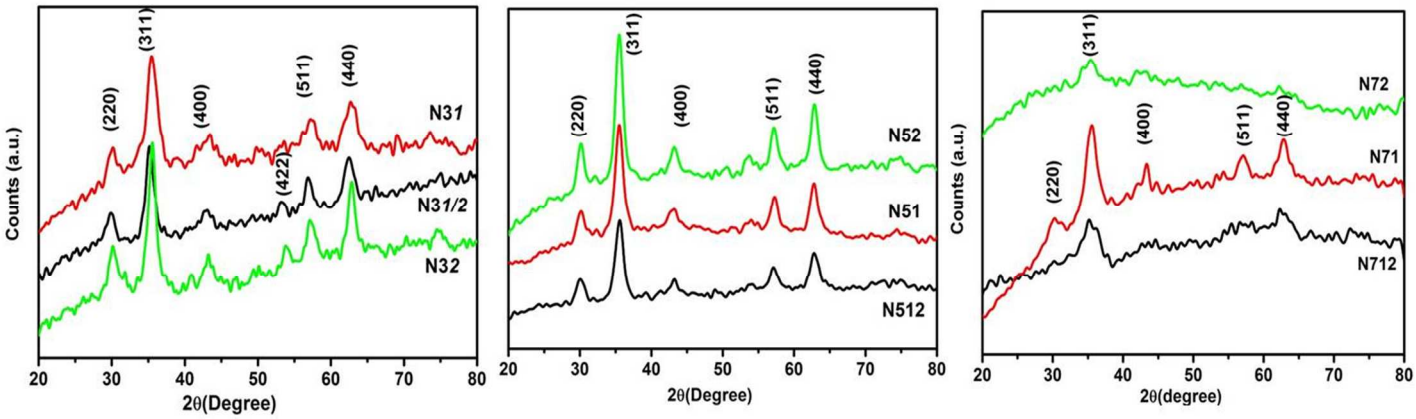

Fig. 2 XRD patterns of Fe_3O_4 NPs at room temperature

The crystallographic structure and phase purity of Fe_3O_4 NPs were investigated by powder XRD. Figure 2. shows the XRD patterns of all the synthesized NPs. All of the NPs exhibited a typical spinel ferrite diffractogram, confirming the expected cubic spinel structure (Fd3m) [21,22]. The average crystallite size D_C was calculated using the Scherrer formula,

$$D_C = \frac{K\lambda}{\beta \cos\theta} \quad (4)$$

where, β is the peak width at half-maximum (FWHM), K is the so-called shape factor which is 0.9 for spherical particles, λ is the wavelength, θ is the Bragg diffraction angle. The

average crystallite sizes of the NPs are calculated from the most intense peak (311) using the said equation. The calculated crystallite size for all samples was below ~10nm (Table 1).

In the present investigation it is found that, as the concentration of the alkaline media DIPA increases from 3M to 5M, there is initial increase in the crystallite size from ~5 nm to ~8 nm. When further increase in the concentration of DIPA to 7M there is broadening of the XRD peaks leads to decrease in crystallite size to ~1 nm. These results are in well accordance with the Mullin [23], where he summarizes that, as the concentration of reacting substances in solution increases, i.e., as the initial supersaturation is increased, the mean size of the precipitate particle increases to a maximum and then decreases. This phenomenon is based on the Weimarn law of precipitation i.e. first law of precipitation, which can be formulated as "With progressively increasing concentration of the reacting solutions, the mean magnitude of the individual crystals of the precipitates will pass through maximum".[24] From this one can conclude that there is direct relation between core size and amine concentration as, core size of NPs travels through maxima with increase in concentration of DIPA.

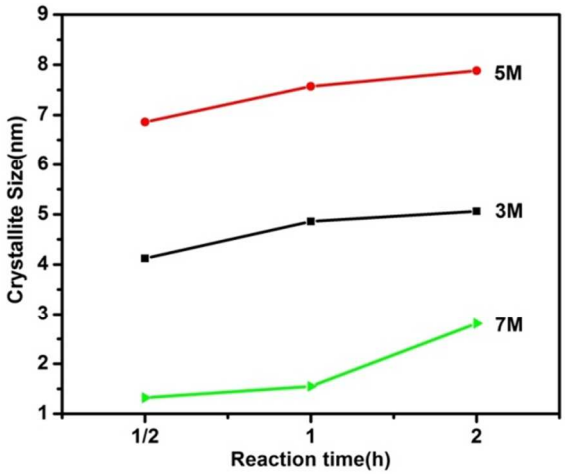

Fig. 3 Variation of crystallite size as a function of reaction time for 3, 5 and 7M concentrations

The crystallite size of the NPs is also influenced by the reaction time. It was found that, the average crystallite size increases from 4.1 nm to 5 nm, 6.8 nm to 7.8 nm and 1.3 nm to 2.8 nm for 3M, 5M and 7M as the reaction time increases from ½ h to 2 h (as shown in Figure 3). This increase in crystallite size with increasing reaction time can directly correlate with the Lifshitz-Slyozov-Wagner (LSW) model for coarsening [14]. According to the simple thermodynamic considerations of Gibbs-Thomson effect [25], coarsening is striving by the

dependence of the solubility of a solid phase on the particle size. Suppose, that the particles are spherical, and then the solubility "Cr" of particles of radius r is,

$$C_r = C_\infty \, exp\left(\frac{2\gamma V_m}{rRT}\right) \quad (5)$$

where C_∞ is the solubility at a flat surface, T is the temperature, γ the surface energy, R the molar gas constant and V_m is the molar volume. For the case where $\left(\frac{2\gamma V_m}{rRT}\right)$ is less than 1, then the exponential term in eq.5 can be linearized and considering the growth is determined by diffusion of the solute from the smaller particles to the larger particles, the subsequent rate law is obtained,

$$\vec{r}^3 - \overrightarrow{r_0}^3 = \frac{8\gamma C_\infty D V_m^2}{9RT} t = At \quad (6)$$

where $\vec{r}$ is the average particle radius at time t and $\vec{r}_0$is the average particle radius at time zero. This model provides a quantitative treatment of the time dependence of the particle size and size distribution [26].

The lattice constants were calculated to be ~8.32 Å for the ½ h reaction time samples N3½, N5½ and N7½ which attributed to the formation of maghemite. As the reaction time increases to 1 h, there is slight change in lattice constant which is about 8.35 Å (considering single phase) which is intermediate between those of maghemite (a = 8.346 Å, JCPDS # 39-1346) and magnetite (a = 8.391 Å JCPDS #19-0629) for all concentration 3, 5 and 7M. This intermediate value of lattice parameter may be due to the presence of large surface energy of particles and the formation of maghemite at the interface of particles because Fe^{2+} ions are more sensitive to oxidation, so ultimately surface ferrous ions can get oxidized to ferric ions which leads to the formation of maghemite. Although all samples prepared at ½ and 1 h reaction time for both 3 and 5M concentration contains characteristics peaks of magnetite, there may be presence of small amount of maghemite (Fe_2O_3) especially at the surface of the particles which is difficult to detect from XRD. These results reveal the presence of both types of iron oxides. Whereas, the lattice parameter determined for all samples having reaction time 2 h in all concentration was to be 8.39 Å, which is in good agreement with the standard value of magnetite 8.39 Å (Table 1). From these observations one can conclude that, along with concentration the reaction time also plays a pivotal role in the formation of iron oxide NPs.

The FT-IR analysis was performed to confirm the formation of iron oxide NPs and to get information about the positions of the ions in the crystal through the vibrational modes. Generally in magnetite, all Fe^{2+} ions occupy octahedral interstices and half of the Fe^{3+} ions

occupy the tetrahedral interstices and remaining half of the Fe^{3+} in octahedral sites. The normal and inverse spinels have four IR bands representing the two fundamentals absorption bands, the first IR fundamental band was due to tetrahedral and second due to octahedral complexes.

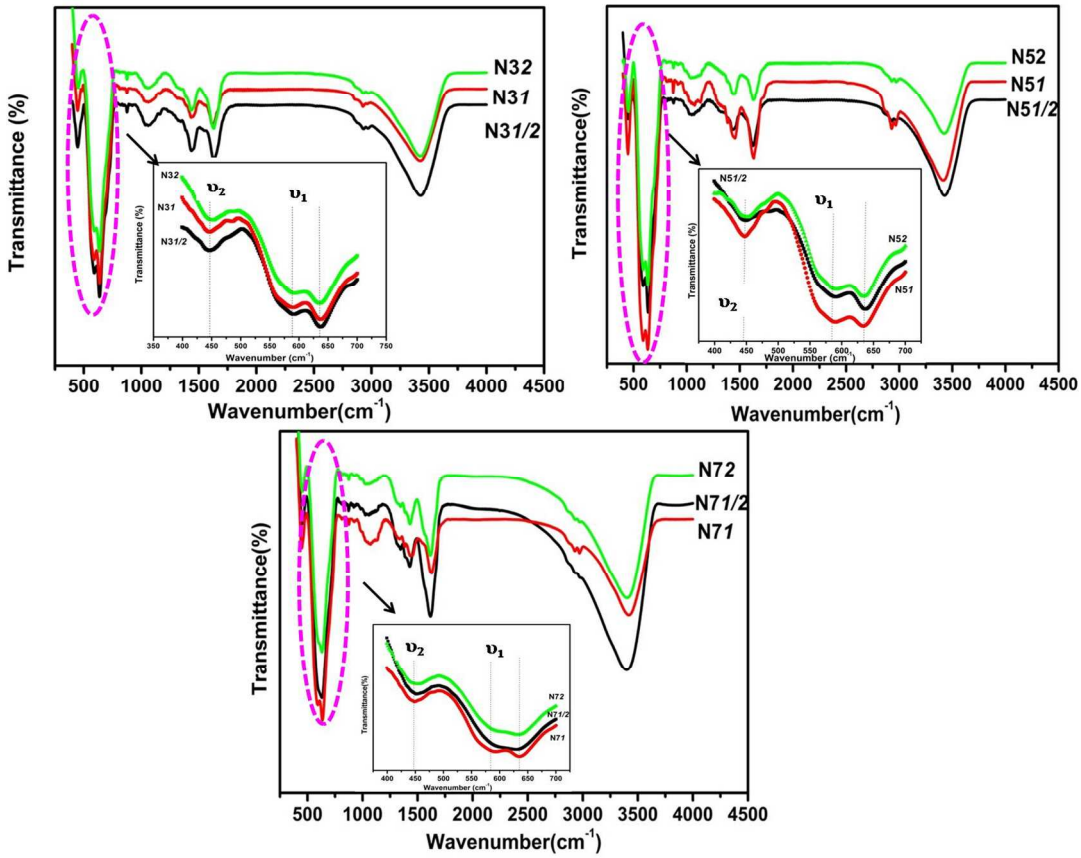

Fig. 4 FT-IR spectra of Fe_3O_4 NPs

The vibration of iron ions in tetrahedral positions was attributed to the high frequency band and low frequency band was attributed to the vibration of iron ions in octahedral positions.[27] The room temperature FT-IR spectra of the as prepared samples are shown in Figure 4. The spectra were recorded in the range from 400 cm^{-1} up to 4000cm^{-1}. According to Waldron [28], the band appeared at 350-450 cm^{-1}(υ_2) is attributed to the stretching vibration of Fe^{3+}–O^{2-} in the octahedral complexes and at 500-600 cm^{-1}(υ_1) to that of bending vibrations in tetrahedral complexes.

From Fig. 4 it is observed that, the FTIR spectra of the Fe_3O_4 NPs exhibits two strong bands one is around 589 cm^{-1} and other one is around 449cm^{-1} assigned to Fe-O stretching vibrations in the tetrahedral and octahedral complexes respectively. Whereas, the stretching vibration of 589 $cm^{-1}$is found with the shoulder around 630 cm^{-1} due to the slight oxidation of the

NPs surface.[13,29] Along with this, various stretching vibrations 650-800 $cm^{-1}$and at around 3300-3500 cm^{-1} were detected for all samples. In which vibrational bands around 3414cm^{-1}, 1615cm^{-1} and 877$cm^{-1}$are attributed to the N-H stretch, N-H bend and N-H wag respectively. While different vibrational bands observed in the range of 1440-1070$cm^{-1}$are corresponds to the C-N stretch and C-C-N bending. All these stretching vibrations are attributed to fingerprint of vibrational modes of DIPA, indicating their adsorption on the surface of the NPs [15].

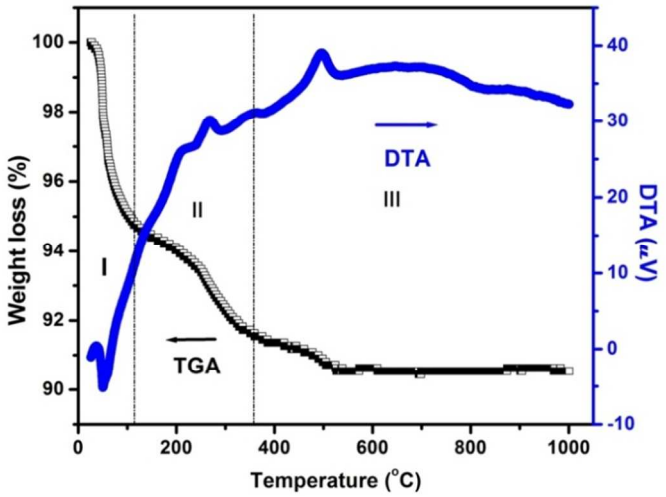

Fig. 5 Typical TG-DTA of the N32 sample

The absorption of DIPA on the surface synthesized Fe_3O_4 NPs are well demonstrated by the TG-DTA. TG-DTA is one of the extremely valuable characterization techniques for thermal characterization of NPs which provides quantitative evidence on the structure of the NPs coating, also allows us to determine the bonding strength of the ligands to the NPs surface and its thermal stability. Typically, ligands that are bound more strongly desorbs at higher temperatures. Figure 5 shows the typical TG-DTA of the N32 sample. From TG-DTA curves it is observed that, there are three major weight loss processes. First step is in between ~30-120˚C, in which there is presence of small endothermic peak below 110˚C accompanied with (3.85%) weight loss, which corresponds to the volatilization of the organic content and to the evaporation of the residual water content. The second and major weight loss process occurs from ~120 to 375˚C with simultaneous exothermic peak at ~270˚C which is attributed to the breakdown of DIPA from the surface of the Fe_3O_4 NPs. This temperature is much higher than the pure DIPA (83˚C, bp). Consequently, temperature shift could be owing to multilayered adsorption of DIPA on the surface of Fe_3O_4 NPs which requires higher temperature for the vaporization of bound DIPA[15].

Third process is in the range ~375- 565˚C at which ~5% weight loss occurs with simultaneous exothermic peak at ~494˚C corresponding to complete decomposition of carbonaceous matter. The strong desorption temperature compared to DIPA is indicative of an increased bonding strength to the NPs surface. This deduction concludes that, there is adsorption of DIPA on the surface of synthesized Fe_3O_4 nanoparticle. [15, 30]

TEM pictures were collected for all Fe_3O_4 NPs synthesized at different Concentrations and reaction time as described in the Experimental section to observe the shape and size of the NPs. Figure 6 show three representative images for N3, N5 and N7 at ½, 1 and 2 h samples respectively. All TEM images show roughly Gaussian-shaped particle size distribution. From TEM pictures it is revealed that, all NPs are nearly spherical in nature, well distributed and slightly in aggregated form. This agglomeration is an indication of exchange of interaction between particles or the high reactivity of the synthesized particles. Histograms of the average diameters were generated from TEM images with the help of ImageJ software. The corresponding distribution histograms are shown in Figure 6. All distributions are unimodal and slightly asymmetrical, with a skewed shape toward the larger areas, characteristic of a lognormal distribution. The average particle size of the NPs is 5.2 nm, 8.5 and 3.2 nm for N3½, N51 and N72 samples respectively which is in well agreement with the particle diameters obtained from XRD data.

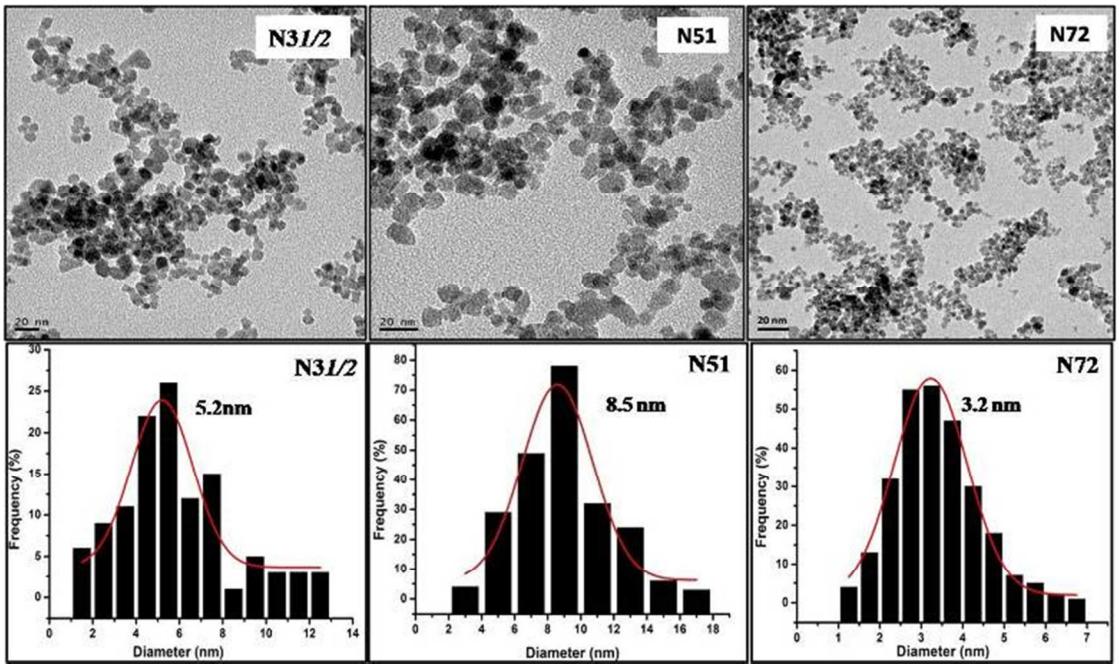

Fig. 6 Representative TEM images and particle size histograms of N3½, N51 and N72 samples

Magnetic properties:

The Figure 7 shows the room temperature hysteresis magnetization of dried samples obtained by SQUID with an applied magnetic field ±15KOe. All samples exhibited superparamagnetic behavior, demonstrating that the thermal energy overcomes the anisotropy energy barrier of a single particle and also the magnetization of nanoparticle assemblage in the absence of an external magnetic field is zero. According to theory of magnetism for exhibiting superparamagnetic behavior, the required minimum nanoparticle volume *Vp* is $25k_B T/K$, where, *K* is the anisotropic constant (for magnetite NPs, $K = -1.1 \times 10^5\ erg/cm^3$), *T* is the room temperature (300 K) and k_B is the Boltzmann constant.[31] If the synthesized NPs assumed to be spherical in nature, in order to exhibit superparamagnetic behavior the diameter of the magnetite NPs should be below 26nm. Our result suggests that, the average size of the all NPs is less than 26 nm. Ultimately, it was expected that all samples should exhibit superparamagnetism.

Table 1. Effect of concentration of DIPA and reaction time on structural properties such as crystallite size observed from XRD (D_C), X-ray density (D_X), Lattice constant (a), Unit cell volume (V), Particle size by TEM (D_{TEM}), magnetic particle size (D_m) by and on magnetic properties as saturation magnetization (M_S), and blocking temperature (τ_B) of Fe_3O_4 NPs.

Sample ID	D_X (gm/cm^3)	a (Å)	V nm^{-3}	D_C (nm)	D_{TEM} (nm)	D_m (nm)	Ms Emu/g	τ_B (K)
N3½	5.35	8.32	0.57	4.12	5.21	2.42	34.33	100.05
N31	5.28	8.35	0.58	4.86	6.33	2.56	37.28	130.00
N32	5.20	8.39	0.59	5.06	7.08	2.78	44.24	140.04
N5½	5.34	8.32	0.57	6.86	7.86	3.07	42.11	150.03
N51	5.27	8.36	0.58	7.57	8.52	3.32	44.16	135.00
N52	5.21	8.39	0.59	7.88	10.14	3.59	60.52	145.04
N7½	5.33	8.32	0.57	1.32	1.99	1.28	11.81	75.00
N71	5.28	8.34	0.58	1.55	2.98	1.49	13.35	78.99
N72	5.20	8.39	0.59	2.81	3.22	2.09	21.67	79.99

The Table 1 shows the value of magnetization (Ms) and blocking temperature (τ_B) etc. It is found that, the magnetic properties of the NPs are also influenced by the effect of reaction time as well as concentration of DIPA. It was observed that, the value of saturation magnetization was increasing from 34.33 to 44.24 emu/g, 42.11 to 60.52emu/g and 11.81 to 21.67 emu/g with increase in reaction time from ½ h to 2 h for 3 M, 5M and 7M concentration respectively. The initial increase and further decrease in saturation magnetization with respect to concentration and ultimately particle diameter suggests a linear dependence of Ms on particle size. Whereas, the value of magnetization for sample N52 is ~ 75% of the bulk Fe_3O_4 NPs (88 emu/g).[32]Such a reduction in magnetization is often observed in NPs and attributed to the finite size effects such as surface spin disorder, spin canting as well as magnetically dead layer on the surface of synthesized NPs.[33] Eventhough, the decrease in value of Ms for all samples is less as compared to bulk, the obtained value of Ms for the particular size is greater than reported earlier.[34] In case of NPs synthesized at 7M concentration, there is diminution in magnetization, which may be due to increase in alkaline media concentration or probability of increase in magnetically dead layer on the surface of NPs.

Using the value of magnetization, magnetic particle size and size distribution can be calculated from following equation,

$$D_m = \left[\frac{18kT}{\pi M_d}\left(\frac{\chi_i}{3\varepsilon M_d H_0}\right)^{1/2}\right]^{1/3} \quad (7)$$

where M_d is the domain magnetization of the bulk Fe_3O_4 (88 emu/g), D_m is the magnetic diameter, χ_i is the initial magnetic susceptibility $\chi_i \sim (dM/dH)H \rightarrow 0$, and ε is the volume fraction of magnetic oxide.Here ε is defined as 1, and H_0 is obtained from the experimental data at a high external field where M versus $1/H$ is linear with an intercept on the M-axis of $1/H_0$. The results of the calculations using only the magnetite phase were listed in table. From Table 1. it was observed that, magnetic particle sizes were showed the same trend (as like D_{XRD} and D_{TEM})i.e. increasing with reaction time, firstly increasing and then decreasing trend with increase in concentration of alkaline media. The size estimations made from magnetic data are slightly lower than the sizes obtained from TEM; this may have come from the magnetically dead surface layer as reported in [35,36].

The study of effect of reaction time and concentration on magnetic properties of synthesized NPs from measurements of the blocking temperature for FC and ZFC processes is an interesting research topic. Zero-field-cooled (ZFC) magnetizations were measured by cooling sample in a zero magnetic field and then increasing the temperature in a static field of 100 Oe, while field-cooled (FC) curves were obtained by cooling the samples in the same static field. Typically in ZFC curve, magnetization increases with temperature and reaches to the maximum at a temperature $\tau_{B,}$ thus it indicates that the magnetic moment of each particle is blocked along its easy magnetization direction at temperature T, which depends on the different physical properties of the particle as particle volume, anisotropy and orientation.

Magnetization as a function of temperature in the applied field of 100 Oe was performed between 5 K and 350 K. From the FC and ZFC curves in Fig. 7(d,e,f), we can observe its irreversibility, typical of the blocking process in superparamagnetic NPs. Furthermore, above the blocking temperature, the magnetization decreases as the temperature increases. From the behavior of the ZFC and FC curves, it is possible to conclude that these curves are almost overlapped above the blocking temperature, τ_B, indicating the presence of the small-sized particles. Also it was observed that, all samples exhibit τ_B at lower temperature i.e. below 200K (listed in Table1) and was influenced by the particle size. It is found that, the ZFC-FC magnetization curves start to diverge near to the τ_B estimated with the ZFC curve. This is due to the relatively narrow size and shape distribution of the sample. It was also observed that τ_B increases with increase in particle size of the NPs, because the distance between the particles is not enough to reduce the dipolar interactions. Indeed, for the iron Oxide NPs, according to the Neel Model transition from the blocked to the superparamagnetic regime occurs at different temperatures for different particle sizes. In the present investigation for all synthesized NPs, the ZFC and FC curves also join together at about τ_B , suggesting that magnetic aggregation is almost not present, in agreement with the individual particle coating and the pseudoself-assembly. Magnetization ZFC curve coincides with that of FC above 150 K. This irreversible behavior is a characteristic of superparamagnetism. [37]

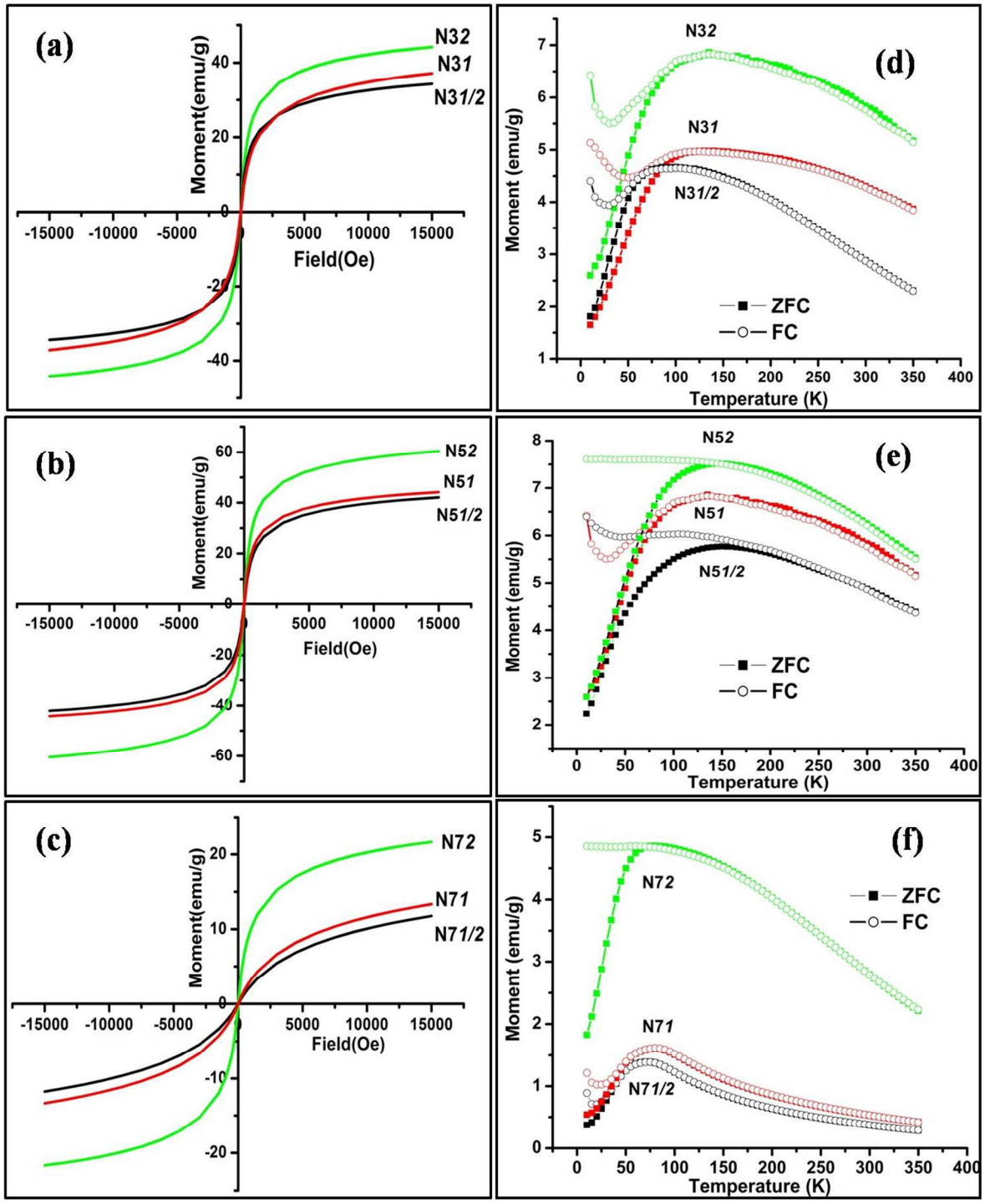

Fig. 7 (a,b,c) Magnetization vs applied magnetic field at room temperature with H up to 15kOe Fe_3O_4 NPs, (d,e,f)Temperature dependence of the magnetization (ZFC and FC) over the temperature range 5−350 K with H = 100 Oe.

Conclusion

This study demonstrates that, the high-yield, one pot synthesis of surface modified Fe_3O_4 NPs accomplished by the co precipitation method. The most interesting result is the effect of concentration of DIPA and reaction time on structural and magnetic properties of precipitated particles. As the concentration of DIPA increases from 3M to 5M the particle size initially increases reaches to its maximum ~4.8nm to ~7.5 nm and then decreases upto ~1.3 nm for 7M concentration. The reaction time required to complete the growth of the Fe_3O_4 NPs is found to be above ½ h. The improved magnetic properties of the Fe_3O_4 NPs are found as compared to the reported in literature. From this study one can conclude that, Can conclude that, the use of DIPA is a potentially very interesting easy route to obtain desirable size and/or magnetic properties of Fe_3O_4 NPs by choosing appropriate parameters

Acknowledgements

Author ABS acknowledge the financial support of Dr. D. Kothari Postdoctoral fellowship program, UGC, INDIA. Author JMR thanks Fundación Ramón Areces for financial support. One of the authors, ABS thanks PEIN Program, Research Excellence Program USC-India.

References

1. N. A. Frey, S. Peng, K. Cheng, S. Sun, *Chem. Soc. Rev*., 2009, **38**, 2532.

2. S. Sun, D. Weller, *J. Magn. Soc. Jpn.*, 2001, **25**, 1434.

3. V. Polshettiwar, R. Luque, A. Fihri, H. Zhu, M. Bouhrara, J. M. Basset, *Chem. Rev.*, 2011, **111,** 3036.

4. K. Mohri, T. Uchiyama, L. V. Panina, *Sens. Actuators A*, 1997, **59**, 1.

5. Jung, J. H.; Lee, J. H.; Shinkai, S. Chem. Soc. Rev. 2011, 40, 4464.

6. A.B. Salunkhe, V.M. Khot, S.H. Pawar, *Current Topics in Med. Chem.,* 2014, **14**, 572.

7. C. S. S. R. Kumar, F. Mohammad, *Adv. Drug Delivery Rev*., 2011, **63**, 789.

8. R. Qiao, C. Yang, M. Gao, *J. Mater. Chem.,* 2009, **19**, 6274.

9. Y. M. Huh, Y. W. Jun, H. T. Song, S. Kim, J. S. Choi, J. H. Lee, S. Yoon, K. S. Kim, J. S. Shin, J. S. Suh, J. Cheon, *J. Am.Chem. Soc.*, 2005, **127**, 12387.

10. H. T. Song, J. S. Choi, Y. M. Huh, S. Kim, Y. W. Jun, J. S. Suh, J. Cheon, *J. Am. Chem. Soc.*, 2005, **127**, 9992.

11. S. Laurent, D. Forge, M. Port, A. Roch, C. Robic, L. V. Elst, R. N. Muller, *Chem. Rev.*, 2008, **108**, 2064.

12 A.K. Gupta, M. Gupta, *Biomater*., 2005, **26**, 3995.

13. C. Pereira, A. M. Pereira, C. Fernandes, M. Rocha, R. Mendes, M. P. Fernández-García, A. Guedes, P. B. Tavares, J. M. Grenèche, J. P. Araújo, C. Freire, *Chem. Mater.*, 2012, **24**,1496.

14. G. Gnanaprakash, J. Philip, T. Jayakumar, B. Raj, *J. Phys. Chem. B*, 2007, **111**, 7978.

15. M. Aslam, E. A. Schultz, T. S. T. Meade, V. P. Dravid, *Crystal Growth & Design*, 2007, **7**, 471.

16. S. Ayyappan, J. Philip, B. Raj, Nanoparticles, Mater. Chem. Phy., 2009, **115**, 712.

17. W. S. Peternele, V. M. Fuentes, M. L. Fascineli, J. R. da Silva, R. C. Silva, C. M. Lucci, R. B. de Azevedo, *J. Nanomater*., 2014, Article ID 682985, http://dx.doi.org/10.1155/2014/682985

18. H. Mehranpour, M. Askari, M. S. Ghamsari. Nucleation and Growth of TiO_2 Nanoparticles, Nanomaterials, Prof. Mohammed Rahman (Ed.), 2011, ISBN: 978-953-307-913-4,

19. I. M. Kolthoff, *J. Phys. Chem.,* 1932, **36**, 860.

20. A. Iqbal, K. Ali, *J. Asian Cera. Soc*., 2013, **1**, 333.

21. D. Caruntu, G. Caruntu, C. J O'Connor, *J. Phys. D: Appl. Phys.,* 2007, **40**, 5801.

22. L. S. Zevin, G. Kimmel, Quantitative X-ray Diffractometry; Mureinik, I., Ed.; Springer-Verlag: New York, 1995

23. J. W. Mullin,. Crystallization, 4th Edition, 2001, Boston, MA, Butterworth-Heinemann ISBN0-7506-4833-3.

24. Weimarn, P.P. von The precipitation laws. *Chem. Reviews*, 1926, **2**, 217-242

25. M. Perez, *Scripta Mater.,* 2005, **52**, 709.

26. G. Oskam, A. Nellore, R. L. Penn, P. C. Searson, *J. Phys. Chem. B,* 2003, **107**, 1734.

27. R.D. Waldron, *Phys. Rev*., 1955, **99,** 1727.

28.B. Zhou, Y. W. Zhang, C. S. Liao, C. H. Yan, L. Y. Chen, S. Y. Wang, J. Magn. Magn. Mater., 2004, **280,** 327.

29. O. Rahman, S. C. Mohapatra, S. Ahmad, Mater. Chem. Phy., 2012,**132**, 196.

30. R. M. Patil, P. B. Shete, N. D. Thorat, S. V. Otari, K. C. Barick, A. Prasad, R. S. Ningthoujam, B. M. Tiwale, S. H. Pawar, J. Magn. Magn. Mater., 2014, **355**, 22.

31. B. D. Cullity, C. D. Graham, Introduction to Magnetic Materials, 2nd Edition, ISBN: 978-0-471-47741-9

32. D. Caruntu, G. Caruntu, C. J O'Connor, *J. Phys. D: Appl. Phys.,* 2007, **40,** 5801

33. A. H. Lu, E. L. Salabas, F. Schth, *Angew. Chem. Int. Ed*. 2007, 46, 1222.

34. (a) S. Wu, A. Sun, F. Zhai, J. Wang, W. Xu, Q. Zhang, A. A. Volinsky, *Mater. Lett.* 2011, **65**, 11882.
(b) K. Petcharoena, A. Sirivat, *Mater. Sci. Engi. B*, 2012, **177,** 421.
(c) M. Tajabadi, M. E. Khosroshahi, *APCBEE Procedia*, 2012, **3**, 140.

35. A. B. Salunkhe, V. M. Khot, N. D. Thorat, M. R. Phadatare, C. I. Sathish, D. S. Dhawale, S. H. Pawar, Appl. Surf. Sci., 2013, **264**,598.

36.V. M. Khot, A. B. Salunkhe, N. D. Thorat, R. S. Ningthoujam and S. H. Pawar, *Dalton Trans.,* 2013, **42**, 1249.

37. Q. Chen, Z. Zhang, *J. Appl. Phys. Lett.* 1998, **73**, 3156.